Hindawi
International Journal of Antennas and Propagation
Volume 2022, Article ID 4038830, 7 pages
https://doi.org/10.1155/2022/4038830

Research Article

Mobile Performance Intelligent Evaluation of IoT Networks Based on DNN

Zhen Tang, Xiaobin Fu, and Pingping Xiao

College of Physical Science and Engineering, Yichun University, Yichun 336000, Jiangxi, China

Correspondence should be addressed to Xiaobin Fu; fxb8508457@163.com

Received 15 December 2021; Revised 14 January 2022; Accepted 21 February 2022; Published 16 March 2022

Academic Editor: Qi Liu

The rapid development of the sensor equipment has promoted the rapid growth of the Internet of Things (IoT). The IoT has been widely employed in the multidimensional signal processing and gradually formed the IoT networks. Mobile communication promotes the wide application of the IoT networks. In this study, the transmit antenna selection (TAS) scheme is employed to investigate the average symbol error probability (ASEP) performance of mobile IoT networks over the 2-Rayleigh channels. We first employ moment-generating function (MGF) approach to derive the exact ASEP expressions. We also investigate the outage probability (OP) performance and derive OP expressions. Employing the deep neural network (DNN), an OP intelligent prediction algorithm is proposed. Then, the numerical simulations are conducted to confirm the ASEP and OP performance analysis. The effect of different channel parameters is also analyzed. Compared with Nakagami and Rayleigh channel models, the 2-Rayleigh model has 83.6% and 59.1% increase in ASEP values, respectively. Compared with ELM and RBF models, the DNN model has 31.7% and 22.5% increase in OP prediction accuracy, respectively.

1. Introduction

In recent years, the information society is facing the transformation from information age to intelligent age. Sensor industry is developing towards the direction of intelligence, low power consumption, and high precision. The intelligent sensor industry plays an important supporting role in the development of the Internet of Things (IoT) and gradually forms the IoT networks [1–3]. With the extensive application of mobile communication, the IoT networks are widely used in transportation, agriculture, and manufacturing [4, 5]. The perspectives and challenges of physical Internet employed in the IoT networks were investigated in [6]. Due to IoT device mobility, the IoT networks are facing many challenges. A new secure user authenticated scheme was employed in the IoT environment to establish a secure transmission process [7]. In the transmission of the biomedical information, smartphone was employed to power the electrochemical biosensing dongle in the IoT networks [8].

Multiple-input multiple-output (MIMO) is an important method to obtain the high data-rate in mobile IoT networks [9]. To improve the system throughput, a Kalman filtering combining scheme was employed in the MIMO system [10]. To improve the power efficiency, the robust beamforming was designed in magnetic MIMO systems [11]. In [12], a deep neural network-based linear precoding method was proposed for multiuser MIMO systems, which can achieve a higher downlink rate. With sparse channels, a low complexity parameter estimation method was proposed for MIMO big data communication system [13]. In [14], the authors considered covert MIMO communications and investigated the covert capacity with variational distance constraint. The sparse Bayesian learning method was used to realize the channel estimation in industrial IoT networks [15].

Transmit antenna selection (TAS) has been widely used in the MIMO system to reduce complexity [16, 17]. With deep neural network, the data-driven prediction method was employed to achieve the TAS in the MIMO system [18]. In

[19], the exact average symbol error probability (ASEP) and outage probability (OP) expressions for underwater MIMO system with TAS were derived. The TAS was employed to improve the ASEP performance of underlay spectrum-sharing MIMO system in [20]. In [21], using the moment-generating function (MGF) method, the TAS scheme was employed to derive the error rate expressions for space-time line code system.

However, the TAS performance of the IoT networks over the 2-Rayleigh channels is very difficult. Motivated by the above discussion, employing TAS and SC schemes, the ASEP and OP performance of the mobile IoT networks is investigated. The main contributions are as follows:

(1) The MGF approach was employed to derive the exact ASEP expressions with TAS, which are used to investigate the ASEP performance of different modulation methods.

(2) Employing the CDF-based approach, the OP expressions are also derived. The derived OP results of the 2-Rayleigh model are more complicated than those of Nakagami and Rayleigh channel models. However, they have a high computational complexity.

(3) Employing the deep neural network (DNN), an OP intelligent prediction algorithm is proposed in this study. The prediction algorithm can achieve rapid analysis of OP performance.

(4) Through different conditions, the effect of different channel parameters is analyzed. Compared with Nakagami and Rayleigh channel models, the 2-Rayleigh model has 83.6% and 59.1% increase in ASEP values. Compared with ELM and RBF models, the DNN model has 31.7% and 22.5% increase in OP prediction accuracy, respectively.

Table 1 shows the notations.

Table 1: Notations.

Notations	Designation
PDF	Probability density function
MSE	Mean square error
SC	Selection combining
CDF	Cumulative density functions
SNR	Signal-to-noise ratio

2. The Mobile IoT Networks

In the mobile IoT networks, it has a mobile source (S) and mobile destination (D). There are K antennas at S and L antennas at D. E_s is the transmit power. Figure 1 shows the system model.

Firstly, Si transmits the signal. The received SNR of Dj is given as

$$\gamma_{ij} = \left|h_{ij}\right|^2 \frac{E_s}{N_0}, \quad i = 1, \ldots, K, j = 1, \ldots, L, \tag{1}$$

where h_{ij} is the channel gain, which follows the 2-Rayleigh model and N_0 is the noise power.

The average SNR is given as

$$\begin{aligned} \overline{\gamma_{ij}} &= E\left(\left|h_{ij}\right|^2\right)\frac{E_s}{N_0} \\ &= E\left(\left|h_{i1}\right|^2\right)e^{-(j-1)W}\frac{E_s}{N_0}, \end{aligned} \tag{2}$$

where W is the power attenuation factor.

Karagiannidis et al. [22] give the CDF and PDF of γ_{ij} as

$$\begin{aligned} F_{\gamma_{ij}}(r) &= G_{1,3}^{2,1}\left[\frac{r}{\overline{\gamma_{ij}}}\middle|_{1,1,0}^{1}\right], \\ f_{\gamma_{ij}}(r) &= \frac{1}{r}G_{0,2}^{2,0}\left[\frac{r}{\overline{\gamma_{ij}}}\middle|_{1,1}^{-}\right]. \end{aligned} \tag{3}$$

D employs the SC combiner, which can select the best γ_{ij}. The output SNR γ_i is

$$\gamma_i = \max\left(\gamma_{i1}, \gamma_{i2}, \ldots, \gamma_{iL}\right). \tag{4}$$

To derive the ASEP and OP results, it needs to obtain the CDF and PDF of γ_i. The CDF of $\gamma_i = \max(\gamma_{i1}, \gamma_{i2}, \ldots, \gamma_{iL})$ is

$$\begin{aligned} F_{\mathrm{SC}}(r) &= \Pr\left[\gamma_i \le r\right] = \Pr\left[\max\left(\gamma_{i1}, \gamma_{i2}, \ldots, \gamma_{iL}\right) \le r\right] \\ &= \prod_{j=1}^{L} \Pr\left[\gamma_{ij} \le r\right] \\ &= \prod_{j=1}^{L} F_{\gamma_{ij}}(r) \\ &= \prod_{j=1}^{L} G_{1,3}^{2,1}\left[\frac{r}{\overline{\gamma_{ij}}}\middle|_{1,1,0}^{1}\right]. \end{aligned} \tag{5}$$

With the derivative of (5), it can obtain the PDF of γ_i

$$f_{\mathrm{SC}}(r) = \sum_{j=1}^{L}\frac{1}{r}G_{0,2}^{2,0}\left[\frac{r}{\overline{\gamma_{ij}}}\middle|_{1,1}^{-}\right] \times \prod_{\substack{p=1 \\ p\neq j}}^{L} G_{1,3}^{2,1}\left[\frac{r}{\overline{\gamma_{ip}}}\middle|_{1,1,0}^{1}\right]. \tag{6}$$

S employs the TAS scheme. For K antennas at S, the g is selected as

$$g = \arg\max\left(\gamma_i\right), \quad 1 \le i \le K. \tag{7}$$

Redha [23] gives the PDF of γ_g

$$f_{\gamma_g}(r) = K\left[F_{\mathrm{SC}}(r)\right]^{K-1} f_{\mathrm{SC}}(r). \tag{8}$$

So, it can obtain the MGF of γ_g [21]:

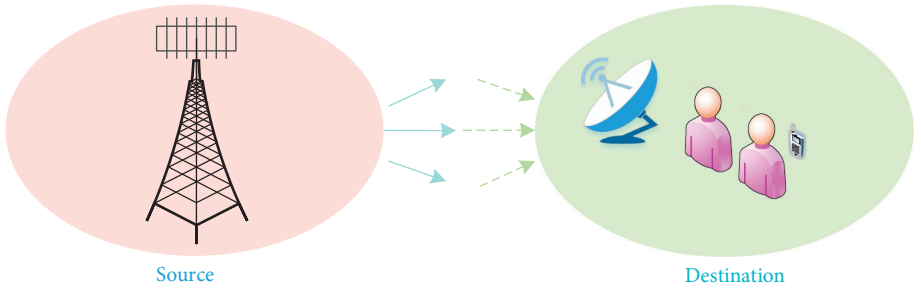

Figure 1: The TAS/SC model.

$$M_{\gamma_g}(s) = \int_0^{\infty} e^{-sr} f_{\gamma_g}(r)\mathrm{d}r = K\int_0^{\infty} e^{-sr} \times \left[\prod_{j=1}^{L} G_{1,3}^{2,1}\left[\frac{r}{\gamma_{ij}}\Big|_{1,1,0}^{1}\right]\right]^{K-1} \times \left(\sum_{j=1}^{L}\frac{1}{r}G_{0,2}^{2,0}\left[\frac{r}{\gamma_{ij}}\Big|_{1,1}^{-}\right] \times \prod_{\substack{p=1\\p\neq j}}^{L} G_{1,3}^{2,1}\left[\frac{r}{\gamma_p}\Big|_{1,1,0}^{1}\right]\right)\mathrm{d}r. \tag{9}$$

3. The ASEP and OP Performance

Yilmaz and Kucur [24] give the ASEP of q-ary PSK:

$$P_{\mathrm{ASEP}} = \frac{1}{\pi}\int_0^{(q-1)\pi/q} M_{\gamma_g}\left(\frac{\sin^2(\pi/q)}{\sin^2\theta}\right)\mathrm{d}\theta. \tag{10}$$

Yilmaz and Kucur [24] give the ASEP of q-ary QAM:

$$PP_{\mathrm{ASEP}} = \frac{4(\sqrt{q}-1)}{\pi\sqrt{q}}\int_0^{\pi/2} M_{\gamma_g}\left(\frac{3}{2(q-1)\sin^2\theta}\right)\mathrm{d}\theta - \frac{4(\sqrt{q}-1)^2}{\pi q}\int_0^{\pi/4} M_{\gamma_g}\left(\frac{3}{2(q-1)\sin^2\theta}\right)\mathrm{d}\theta. \tag{11}$$

The OP is

$$\begin{aligned} P_{\mathrm{out}} &= \Pr\left[\gamma_g \le r_{\mathrm{th}}\right] \\ &= \Pr\left[\arg\max_{1\le i\le K, 1\le j\le L}\left(\gamma_{ij}\right) \le r_{\mathrm{th}}\right] \\ &= \prod_{i=1}^{K}\prod_{j=1}^{L}\Pr\left[\gamma_{ij} \le r_{\mathrm{th}}\right] \\ &= \prod_{i=1}^{K}\prod_{j=1}^{L}\int_0^{r_{th}} f_{\gamma_{ij}}(r)\mathrm{d}r, \end{aligned} \tag{12}$$

where r_{th} is a given threshold.

Employing (3) and (4), it can obtain the OP as

$$P_{\mathrm{out}} = \prod_{i=1}^{K}\prod_{j=1}^{L} G_{1,3}^{2,1}\left[\frac{r_{\mathrm{th}}}{\gamma_{ij}}\Big|_{1,1,0}^{1}\right]. \tag{13}$$

4. OP Prediction Algorithm

However, (14) has a high computational complexity. In order to realize real-time analysis of OP performance, we propose an OP prediction method based on DNN.

From (13), K, L, r_{th}, and W constitute the DNN input X. The DNN output y is P_{out}.

The DNN structure is shown in Figure 2. It has six layers, which are input layer, two hidden layers, ReLU layer, sigmoid layer, and output layer, respectively.

For the input layer, it has four characteristics. Then, it uses full connection to connect with two hidden layers. The hidden layers have 512 and 1024 neurons, respectively. Meanwhile, we use ReLU and Sigmoid functions after hidden layer 1 and hidden layer 2, respectively. To make regression prediction, Sigmoid function is employed to finally predict the output.

MSE is widely used as an evaluation criterion in deep learning. So, we also employ the MSE to evaluate the OP prediction effect. MSE is given as [16, 17]

$$\mathrm{MSE} = \frac{\sum_{i=1}^{S}(t_i - y_i)^2}{S}, \tag{14}$$

where t_i is the predicted output and S is the number of the testing date.

5. Simulation Analysis

Figures 3 and 4 present the impact of W on the ASEP and OP performance, respectively. The parameters are in Table 2. We can obtain that the ASEP and OP performance is degraded as W increases. For example, when SNR = 16 dB, the W values are 0.5, 2, and 4, respectively, the ASEP values are 9×10^{-4},

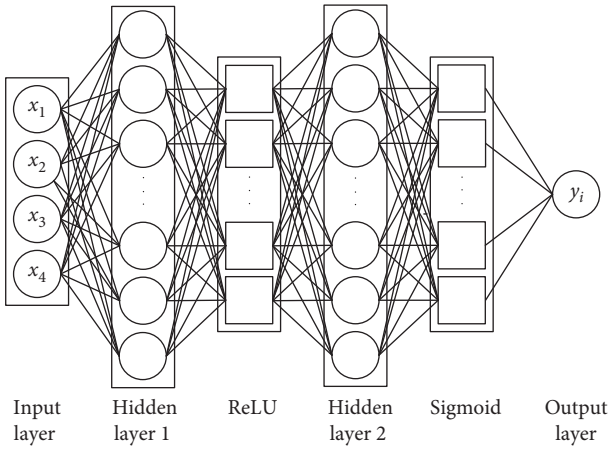

Figure 2: The DNN structure.

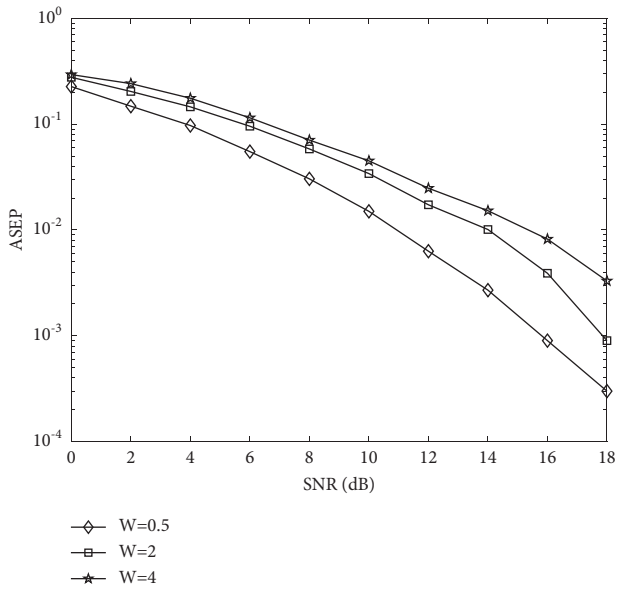

Figure 3: The ASEP performance with different (W).

3.9×10^{-3}, and 8.2×10^{-3}, respectively. With W increases, the fading severity is more serious.

Figure 5 presents the ASEP performance comparison. We can obtain that the ASEP performance of the 2-Rayleigh model is worse than that of Rayleigh and Nakagami models. When SNR = 10 dB, the ASEP values are 0.0450, 0.0184, and 0.0074, respectively. Compared with Rayleigh and Nakagami channel models, the 2-Rayleigh model has a 59.1% and 83.6% increase in ASEP values, respectively. This shows that the communications environment of the 2-Rayleigh model is more complex than that of Rayleigh and Nakagami models.

Figure 6 presents the OP performance comparison. When SNR = 6 dB, the OP values are 0.3214, 0.1902, and 0.0968, respectively. Compared with Nakagami and Rayleigh channel models, the 2-Rayleigh model has a 69.9% and 49.1% increase in OP values, respectively.

For the DNN, ELM, and RBF algorithms, Figures 7–9 show the prediction results, and Table 3 shows the

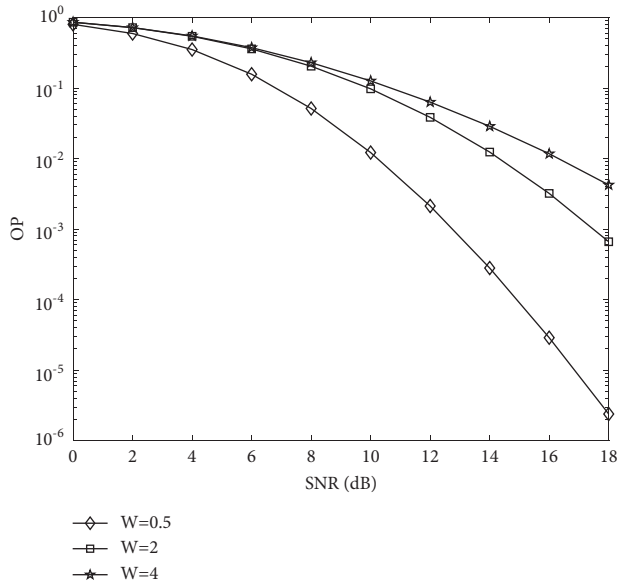

Figure 4: The OP performance with different (W).

Table 2: Simulation parameters for Figures 3–6.

Parameters	Value
E	1
W	0.5, 2, 4
K	2
L	2
γ_{th}	5 dB

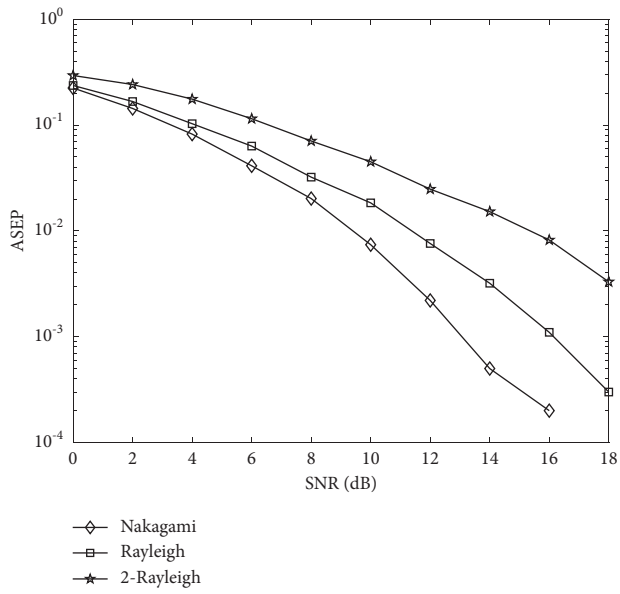

Figure 5: The ASEP performance comparison with different channel models.

simulation parameters. The prediction results of the DNN algorithm are better than ELM and RBF methods. Table 4 shows the MSE comparison. The MSE with the DNN

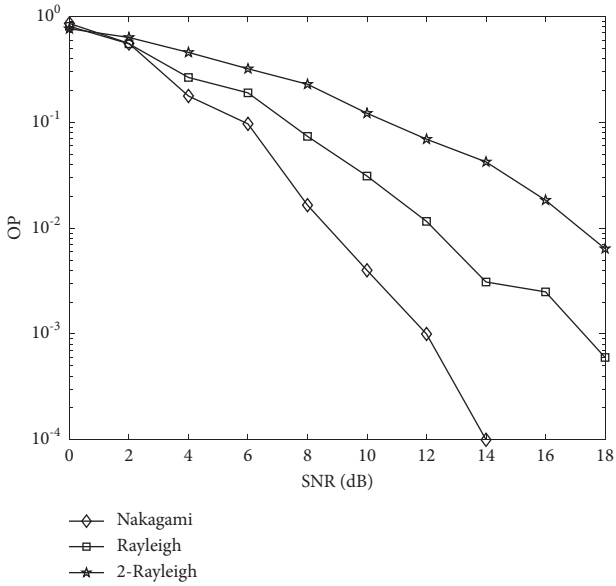

Figure 6: The OP performance comparison with different channel models.

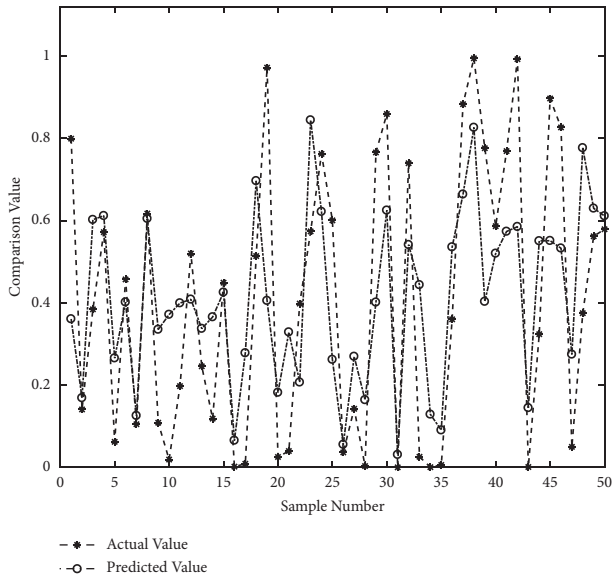

Figure 7: DNN prediction.

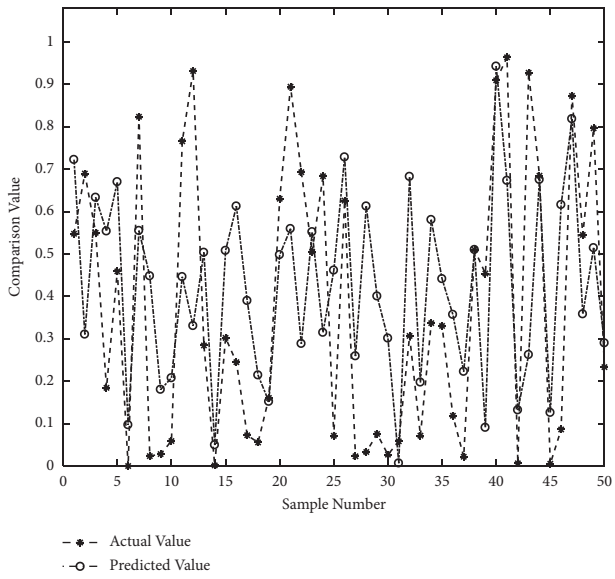

Figure 8: ELM prediction.

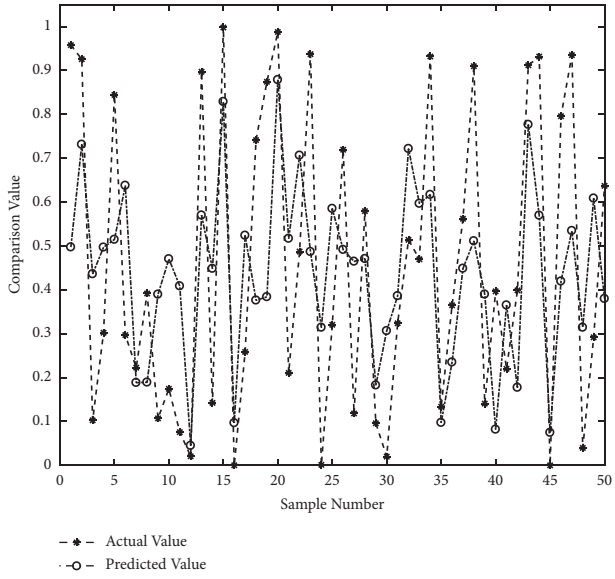

Figure 9: RBF prediction.

Table 3: Simulation parameters for Figures 7–9.

Parameters	DNN	ELM	RBF
	Training set: 1120; testing set: 50		
	X:4	X:4	X:4
	y:1	y:1	y:1
	q: [512, 1024]	q:[100]	q:[120]
	lr: 0.00024		

Table 4: MSE comparison for the three algorithms.

Algorithms	MSE
DNN	0.0557
ELM	0.0815
RBF	0.0719

algorithm is only 0.0557, which is lower than ELM and RBF methods. Compared with ELM and RBF models, the DNN model has 31.7% and 22.5% increase in OP prediction accuracy, respectively.

6. Conclusions

We investigated the ASEP and OP performance of the 2-Rayleigh model, respectively. Through different conditions, the effect of K, L, and W on the ASEP and OP performance was analyzed. K or L values increased, and the system performance was improved. The ASEP and OP performance degraded as W increased. Compared with Nakagami and Rayleigh channel models, the 2-Rayleigh model had 83.6% and 59.1% increase in ASEP values, respectively. The DNN model had a better OP prediction accuracy than the ELM and RBF algorithms.

Data Availability

The data used to support the findings of this study are available from the corresponding author upon reasonable request and with permission of funders.

Conflicts of Interest

The authors declare that they have no conflicts of interest.

Acknowledgments

This project was supported by the National Natural Science Foundation of China (no. 11664043).

References

[1] L. Xu, X. Zhou, Y. Tao, L. Liu, X. Yu, and N. Kumar, "Intelligent security performance prediction for IoT-enabled healthcare networks using an improved CNN," *IEEE Transactions on Industrial Informatics*, vol. 18, no. 3, pp. 2063–2074, 2022.

[2] H. Wang, P. Xiao, and X. Li, "channel parameter estimation of mmWave MIMO system in urban traffic scene: a training channel-based method," *IEEE Transactions on Intelligent Transportation Systems*, pp. 1–9, 2022.

[3] L. Xu, H. Wang, and T. A. Gulliver, "Outage probability performance analysis and prediction for mobile IoV networks based on ICS-BP neural network," *IEEE Internet of Things Journal*, vol. 8, no. 5, pp. 3524–3533, 2021.

[4] X. P. Wang, L. T. Yang, D. D. Meng, M. Dong, K. Ota, and H. Wang, "Multi-UAV Cooperative Localization for Marine Targets Based on Weighted Subspace Fitting in SAGIN Environment," *IEEE Internet of Things Journal*, 2022.

[5] H. Wang, W. C. Du, X. P. Wang, and L. W. Xu, "Channel estimation performance analysis of FBMC/OQAM systems with bayesian approach for 5G-enabled IoT applications," *Wireless Communications and Mobile Computing*, vol. 2020, Article ID 2389673, 9 pages, 2020.

[6] H. Tran-Dang, N. Krommenacker, P. Charpentier, and D.-S. Kim, "Toward the Internet of Things for physical Internet: perspectives and challenges," *IEEE Internet of Things Journal*, vol. 7, no. 6, pp. 4711–4736, 2020.

[7] A. Jabbari and J. B. Mohasefi, "A secure and LoRaWAN compatible user authentication protocol for critical applications in the IoT environment," *IEEE Transactions on Industrial Informatics*, vol. 18, no. 1, pp. 56–65, 2022.

[8] J. Guo, "Smartphone-powered electrochemical biosensing dongle for emerging medical IoTs application," *IEEE Transactions on Industrial Informatics*, vol. 14, no. 6, pp. 2592–2597, 2018.

[9] H. Wang, L. Wan, M. Dong, K. Ota, and X. Wang, "Assistant vehicle localization based on three collaborative base stations via SBL-based robust DOA estimation," *IEEE Internet of Things Journal*, vol. 6, no. 3, pp. 5766–5777, 2019.

[10] S. Park, "Kalman filtering based combining for MIMO systems with hybrid ARQ," *IEEE Transactions on Signal Processing*, vol. 69, no. 9, pp. 5250–5258, 2021.

[11] Y. Zhang, D. Chen, and T. Jiang, "Robust beamforming design for magnetic MIMO wireless power transfer systems," *IEEE Transactions on Signal Processing*, vol. 69, no. 9, pp. 5066–5077, 2021.

[12] K. Kong, W. J. Song, and M. Min, "Knowledge distillation-aided end-to-end learning for linear precoding in multiuser MIMO downlink systems with finite-rate feedback," *IEEE Transactions on Vehicular Technology*, vol. 70, no. 10, Article ID 11095, 2021.

[13] H. Wang, L. Xu, Z. Yan, and T. A. Gulliver, "Low-complexity MIMO-FBMC sparse channel parameter estimation for industrial big data communications," *IEEE Transactions on Industrial Informatics*, vol. 17, no. 5, pp. 3422–3430, 2021.

[14] S.-Y. Wang and M. R. Bloch, "Covert MIMO communications under variational distance constraint," *IEEE Transactions ;on Information Forensics and Security*, vol. 16, no. 9, pp. 4605–4620, 2021.

[15] H. Wang, X. Li, R. H. Jhaveri et al., "Sparse bayesian learning based channel estimation in FBMC/OQAM industrial IoT networks," *Computer Communications*, vol. 176, pp. 40–45, 2021.

[16] L. Xu, X. Yu, and T. A. Gulliver, "Intelligent outage probability prediction for mobile IoT networks based on an IGWO-elman neural network," *IEEE Transactions on Vehicular Technology*, vol. 70, no. 2, pp. 1365–1375, 2021.

[17] L. W. Xu, X. P. Zhou, X. W. Li, R. H Jhaveri, T. R. Gadekallu, and Y. Ding, "Mobile collaborative secrecy performance prediction for artificial IoT networks," *IEEE Transactions on Industrial Informatics*, 2021.

[18] H. Liu, Y. Xiao, P. Yang, J. Fu, S. Li, and W. Xiang, "Transmit antenna selection for full-duplex spatial modulation based on machine learning," *IEEE Transactions on Vehicular Technology*, vol. 70, no. 10, pp. 10695–10708, 2021.

[19] I. S. Ansari, L. Jan, Y. T. Tang, L. Yang, and M. H. Zafar, "Outage and error analysis of dual-hop TAS/MRC MIMO RF-UOWC systems," *IEEE Transactions on Vehicular Technology*, vol. 70, no. 10, pp. 10695–10708, 2021.

[20] R. Sarvendranath and N. B. Mehta, "Statistical CSI driven transmit antenna selection and power adaptation in underlay spectrum sharing systems," *IEEE Transactions on Communications*, vol. 69, no. 5, pp. 2923–2934, 2021.

[21] S. C. Lim and J. Joung, "Transmit antenna selection for space-time line code systems," *IEEE Transactions on Communications*, vol. 69, no. 2, pp. 786–798, 2021.

[22] G. K. Karagiannidis, N. C. Sagias, P. T. Mathiopoulos, and N. Nakagami, "A novel stochastic model for cascaded fading channels," *IEEE Transactions on Communications*, vol. 55, no. 8, pp. 1453–1458, 2007.

[23] M. R. Redha, "Impact of delayed arbitrary transmit antenna selection on the performance of rectangular QAM with receive MRC in fading channels," *IEEE Communications Letters*, vol. 13, no. 6, pp. 390–392, 2009.

[24] F. Yilmaz and O. Kucur, "Exact performance of wireless multi-hop transmission for M-ary coherent modulations over generalized gamma fading channels," in *Proceedings of the 2008 IEEE 19th International Symposium on Personal, Indoor and Mobile Radio Communications*, pp. 1–5, Cannes, France, September 2008.